We are IntechOpen,
the world's leading publisher of
Open Access books
Built by scientists, for scientists

6,900
Open access books available

186,000
International authors and editors

200M
Downloads

Our authors are among the

154
Countries delivered to

TOP 1%
most cited scientists

12.2%
Contributors from top 500 universities

CLARIVATE ANALYTICS
BOOK CITATION INDEX
INDEXED

WEB OF SCIENCE™

Selection of our books indexed in the Book Citation Index
in Web of Science™ Core Collection (BKCI)

Interested in publishing with us?
Contact book.department@intechopen.com

Numbers displayed above are based on latest data collected.
For more information visit www.intechopen.com

Chapter

Long-Distance LIDAR Mapping Schematic for Fast Monitoring of Bioaerosol Pollution over Large City Areas

Dimitar Stoyanov, Ivan Nedkov, Veneta Groudeva,
Zara Cherkezova-Zheleva, Ivan Grigorov, Georgy Kolarov,
Mihail Iliev, Ralitsa Ilieva, Daniela Paneva
and Chavdar Ghelev

Abstract

Light detection and ranging (LIDAR) atmospheric sensing is a major tool for remote monitoring of aerosol pollution and its propagation in the atmosphere. Combining LIDAR sensing with ground-based aerosol monitoring can form the basis of integrated air-quality characterization. When present, biological atmospheric contamination is transported by aerosol particles of different size known as bioaerosol, whose monitoring is now among the basic areas of atmospheric research, especially in densely-populated large urban regions, where many bioaerosol-emitting sources exist. Thus, promptly identifying the bioaerosol sources, including their geographical coordinates, intensities, space-time distributions, etc., becomes a major task of a city monitoring system. This chapter argues in favor of integrating a LIDAR mapping schematic with in situ sampling and characterization of the bioaerosol in the urban area. The measurements, data processing, and decision-making aimed at preventing further atmospheric contamination should be performed in a near-real-time mode, which imposes certain demands on the typical LIDAR schematics, including long-range sensing as a critical parameter, especially over large areas (10 – 100 km2). In this chapter, we describe experiments using a LIDAR schematic allowing near-real-time long-distance measurements of urban bioaerosol combined with its ground-based sampling and physicochemical and biological studies.

Keywords: LIDAR monitoring , particulate matter, atmospheric pollution, contaminations

1. Introduction

Atmospheric aerosol pollution or more appropriately particulate matter (PM) is key subject for the human health and ecosystem stability. At present, more than 2000 papers are published per year addressing research topics related to

atmospheric aerosols [1]. However, surprisingly little is known regarding the genesis, composition, or dynamics of the atmosphere's microbial inhabitants, particle's chemical composition, particle's surface pollution, and their relation with the PM [2, 3]. In what concerns human health, the most harmful ones are the particles with sizes below 10 µm, standardized in terms of permissible concentration as $PM_{2.5}$ and PM_{10}. The fast pace of the information technology development in the first decade of twenty-first century created extraordinary possibilities for organizing systems for real-time monitoring of the atmosphere over urban areas. The implementation of such techniques requires the development of modern fast sensor systems, whose principle of operation, size, and convenient management ensures a problem-free functioning of the information systems without affecting the life in the particular urban area. The well-known techniques of PM monitoring include as a rule a small number of stations and the use of specialized algorithms for rapid assessment of the aerosol pollution's spatial structure above the city. These approaches suffer from a number of drawbacks, such as limited spatial resolution as compared with the urban structure, the low temporal resolution from the viewpoint of the quick polluting processes, and following the PM proliferation, the use of non-calibrated devices, and the subjectivity in selecting the sampling sites. A major drawback of the techniques in question is the relatively slow determination of the pollution sources. Of particular interest in assessing the air quality in urban areas is the biological contamination transported by PM in the form of bioaerosols. According to [4], almost 25% of the total airborne PM above land surfaces contains biological materials in the form of pollens, fungal spores, bacteria, viruses, and fragments from plants, animals, or living organisms with a size ranging from 0.02 up to 100 µm [5–8].

The present chapter discusses the capabilities of remote techniques of analyzing the pollution fields in conjunction with in situ sampling of bioaerosols and investigation of PM pollution as one of the promising approaches to raising the efficiency of systems of air monitoring over urban areas [9–11]. The light detection and ranging (LIDAR) techniques are considered as being among the ones best suited to real-time scanning and/or long-term monitoring of the pollution above large areas. Their advantages arise from several factors: (1) light wavelengths commensurate with or close to the PM size, (2) good resolution in terms of distance (5–30 m) and elevation angle (~1°), and (3) range of operation (20–30 km) [12]. In a scanning mode of operation, the LIDAR techniques allow one to construct LIDAR maps of the aerosol pollution distribution over large cities, which can be easily juxtaposed with the ground atmospheric monitoring networks. Special attention was paid here to the development of a specific LIDAR measurement schematic to be suitably combined with in situ bioaerosol sampling investigating its crystallo-chemical and surface structure, including the presence of bacteria and adsorbed nano- and micron-sized organic and inorganic contamination. The successful applicability of such combined methodology is demonstrated below by the results of a study of the PM size distribution and genesis in two typical urban zones within a large city (Sofia, capital of Bulgaria, population of approx. 1.3 million), in places where the LIDAR monitoring had established previously a mass concentration in peak hours of vehicle traffic.

1.1 LIDAR technologies applied in aerosol sensing

In the literature [13] one can find descriptions of various LIDAR techniques based on the interaction of laser radiation with bioaerosols, such as Mie, Rayleigh,

and Raman [9, 10] scattering and laser-induced fluorescence of bioaerosols [14]. Depolarization LIDAR techniques are also employed, whereby measuring the laser light depolarization, and based on models of non-spherical aerosols, the latter's origin can be distinguished, e.g., dust, smoke, pollen, including bioagents as anthrax, ricin, etc.

The Mie scattering-based LIDAR techniques of bioaerosol remote sounding allow one to use simple and inexpensive LIDAR equipment efficient in long-distance vertical and horizontal scanning. Moreover, these LIDARs easily provide long-distance operation exceeding 30–50 km [9, 10] and 25 km by our LIDAR system [11]. A drawback of this approach arises when one needs a more detailed aerosol fields' characterization in terms of size distribution, non-sphericity or spectral properties of the particles. To satisfy such requirements, various more complex techniques had been developed. For example, UV laser-induced fluorescence allows one to assess the particles' elemental composition based on their electron and rotational-vibrational spectra [15]. The Raman IR spectroscopy technique provides information on the rotational-vibrational spectra of the molecular compounds constituting the particles. The differential absorption LIDAR (DIAL) techniques are also used to determine the presence of gaseous species in the atmosphere based on the absorption of specific laser light wavelengths [16].

The high degree of informativeness of these complex techniques from the viewpoint of a detailed bioaerosol description cannot, unfortunately, be combined with other requirements of importance for their efficient inclusion in networks for air-quality monitoring of the low atmosphere in urban areas. Here we will point out just the more important constraints: (i) high technical complexity, size, and cost of the LIDAR systems; (ii) short operative distances (2–5 km), seriously limiting the possibility of implementing bioaerosol monitoring system in large cities; and (iii) using the laser radiation focusing on the aerosol particles, etc.

The purpose of our investigations described below was to explore experimentally the possibility to make use of Mie scattering in a relatively simple LIDAR configuration emitting horizontally the near-ground atmosphere, thereby sounding from a single point the territory of a large city with high angular and distance resolutions. We present successively the LIDAR and sampling equipment in their concurrent functioning, as well as the results of the structural and biological studies, thus proving the capabilities of the LIDAR biomonitoring technique functioning within an urban air-quality monitoring and information system.

1.2 Methodology of combined LIDAR bioaerosol measurements

The methodology for performing the combined LIDAR bio-measurements, capable to be applied in near real-time regimes, is illustrated in **Figure 1**. In general its operation is based on the use of two independent subsystems: (i) LIDAR long-distance sensing subsystem, containing scanning LIDAR for fast 3D mapping aerosol fields (distance, time, mass concentration), and (ii) aerosol sampling equipment of the aerosol particles, transporting bio-contaminations disposed near the LIDAR illuminated resolution volume. The sampled bioaerosol particles are then processed by different methods and algorithms for determination of the mass concentration and LIDAR calibration, bio-contaminant characterization by different techniques, etc. The fast processing of calibrated LIDAR data provides opportunities for
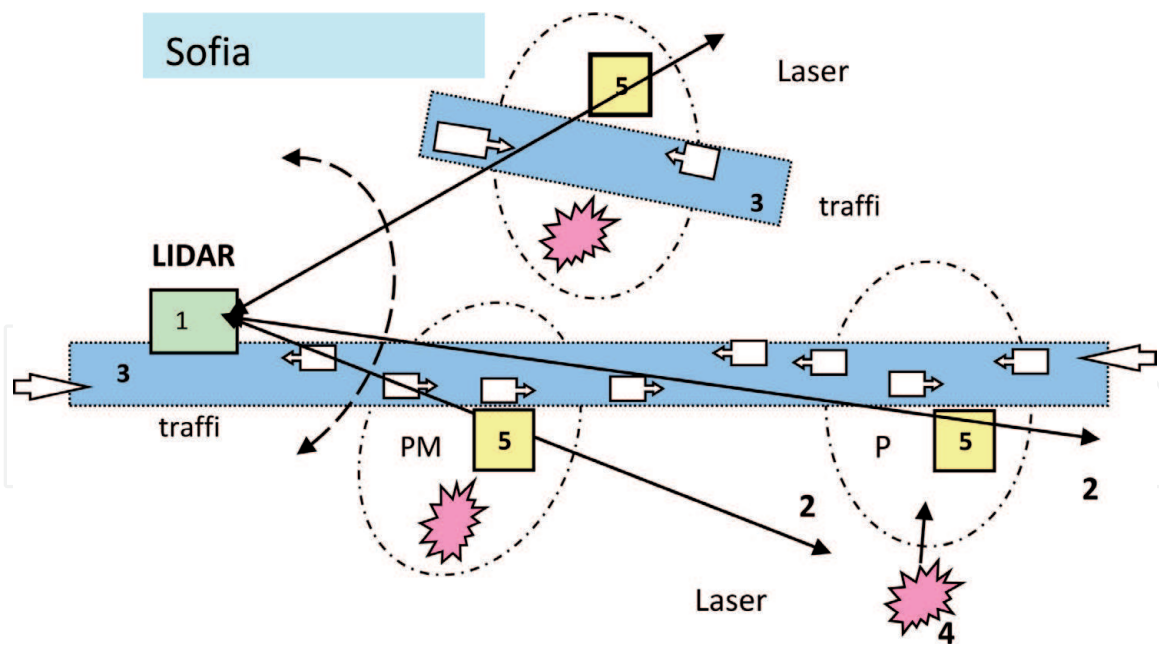
Figure 1.
Schematic diagram of a LIDAR bioaerosol measurement system.

well-timed decision-making for prevention of further spreading of bio-pollutants over the entire city area.

The LIDAR equipment is disposed in a single point (1). The laser beam is directed along specific paths (2) partly overlapping major city thoroughfares (3) with heavy traffic. These directions are selected on the basis of preliminary estimates (by, e.g., city monitoring network) of the presence of localized sources (4) emitting bio-contaminants that are subsequently transported in the near-ground atmosphere by PM. The PM sampling equipment (5) is placed close to the heavy-traffic spots, as explained below. In this schematic the scanning LIDAR capabilities could provide an effective coverage of too large areas of radius up to 25 km (1000 km^2 and more).

1.2.1 LIDAR sensing subsystem

LIDAR sensing subsystem for mapping the aerosol field above the sampling device (5) (**Figure 1**). An important point here is the contribution of the automobile traffic creating sufficiently strong backscattered LIDAR signals due to the PM, emitted by internal combustion engines. As these are formed at high tempera-tures, the possibility of its initially containing microorganisms is negligible. The hot PMs are then lifted up quickly in the air and enter the field of proliferation of bio-contaminants originating from the sources (4) (**Figure 1**). Thus, PM serves as a transport medium for the bioaerosols spreading over the city. In hours of heavy traffic, the backscattered LIDAR signal from bioaerosol-bearing PM is strong enough to allow remote sounding to distances of up to 10 km and more. After a fast computer processing, the LIDAR maps constructed can directly be used by the air-quality monitoring systems.

1.2.2 Sampling subsystem

It is described in detail below when we analyze the bio-contaminants found in the LIDAR sounding zones. The sampling is independent of the LIDAR sub-system, but it is important to synchronize the sampling time and duration with the LIDAR sounding in the vicinity of the sampling site. The LIDAR map can be used (with the aid of specialized algorithms) to establish the probable locations

of sources of PM and bio- and other pollutants. The sampling data allow us to calibrate the LIDAR signal in terms of mass concentration (see below), thus shortening the time of reaction to the appearance of PM and other pollutants based on LIDAR observations only. We should note here that the delay due to processing the results as compared with the time necessary to process the LIDAR data (nearly real time) will not cause problems in the functioning of the entire system together with the city monitoring system. The sampling data will be saved and documented and could thus be used at a later stage.

2. Techniques and equipment

2.1 LIDAR subsystem

The LIDAR subsystem used in the experiments described here is of the scanning type with capability of scanning the entire hemisphere with an angular resolution of ~1° and is part of the EARLINET and ACTRIS LIDAR Station of Institute of Electronics—Bulgarian Academy of Sciences (IE-BAS) (see **Figure 2a**). It has been, and is, used in a large number of experiments of observation, monitoring, and mapping of the transport (including the transborder) of aerosol loadings over the city of Sofia [15]. The emitter is a CuBr vapor laser, with an output power of 2–4 W, pulse repetition rate of 5–10 kHz, and pulse duration of ~10 ns, the probing wavelength emitted being 510.6 nm. The receiving part operates in a photon-counting mode allowing sounding at distances up to $R_{max} \sim 25$–30 km [11]. The diameter of the Cassegrain-type receiving telescope is 19 cm. The LIDAR profiles are recorded and processed by a computer by the known algorithms [17, 18] and are then presented as multidimensional (depending on the sounding geometry) LIDAR maps. The laser beam divergence after collimation is within 1–2 mrad and can be varied if necessary. The receiving angle of the optical system can also be varied by varying the diameter of the diaphragm in front of the photon counter. Further, the spatial resolution is chosen within the 15–30 m range (usually 30 m); thus, the scattering volume is about twice as large as the volume pumped during the time of measurement by the aerosol sampler located nearby.

Figure 2b presents a vertical cross section of the atmosphere with origin at the LIDAR station and directed to downtown Sofia along the city's main thoroughfare, Tsarigradsko Chaussee Blvd. One clearly sees the vertical structure of the atmospheric aerosol density (in terms of backscatter coefficient), comprising a well-expressed ground layer with a height of 500–600 m, together with other

a)   b)   c)
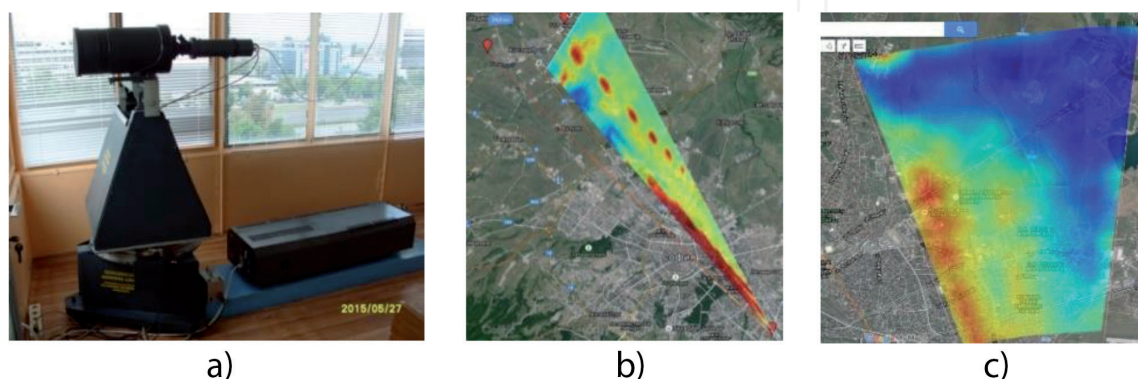
Figure 2.
(a) Cu vapor LIDAR for atmospheric scanning; (b) LIDAR map of a vertical cross section of the atmosphere with origin at the IE-BAS LIDAR Station; (c) LIDAR map of the near-ground atmosphere of a city zone with high and low degree of PM pollution color-coded by brown and blue, respectively.

aerosol formations of limited size. The aerosol loading of the near-ground layer over the urbanized part of Sofia City Municipality is due to various sources (both local and transborder), with the main one being heavy automobile traffic, which is the subject of the present discussion. **Figure 2c** is a LIDAR map of part of the urban area, where one can see again well-defined zones of high (brown) and low (blue) MP pollution.

2.2 Calibration of LIDAR extinction and backscattering coefficients

Analyzing the PM aerosol loadings formed in the vicinity of heavy-traffic urban areas and experimentally measured by the LIDAR technique schematically presented in **Figure 2**, we were able to draw the important conclusion that the mass concentration of the aerosol loading of hot PM emitted by internal combustion engines is a key parameter when one applies a LIDAR-based methodology to air-quality monitoring in a large city. We thus calibrated the two major LIDAR parameters, namely, the extinction coefficient $\alpha(r)$ and the backscatter coefficient $\beta(r)$, in terms of the aerosol mass concentration following the well-known method [17, 19] and making use of the mass concentration M_a data obtained by the sampling device. For the LIDAR ratio $LiR = \alpha(r)/\beta(r)$, we adopted the typical value of $LiR = 50$ [16, 19]. The parameters $\beta(r)$ and $\alpha(r)$ were calculated using the LIDAR equation under the assumption of a horizontally homogeneous atmosphere:

$$P(r) = P_0 \frac{c\tau}{2} C \frac{\beta(r)}{r^2} exp\left[-2\int_{r_0}^{r}\alpha(r)dr\right] \tag{1}$$

where $P(r)$ is the power of the detected laser radiation backscattered from the atmosphere from a distance $r = \frac{ct}{2}$ after a period of time t following the moment of laser pulse emission and τ is the pulse duration. Under the homogeneity assumption, the extinction coefficient $\alpha(r)$ is calculated as.

$$\alpha(r) = -\frac{1}{2}\frac{dS(r)}{dr}, \text{where } S(r) = \ln\left[r^2 P(r)\right] \tag{2}$$

Figure 3a and **b** presents the calibration dependencies of the mass concentration in [mg/m^3] of, respectively, $\alpha(r)$ and $\beta(r)$. In both cases, the linear fit (Y = A + B.x) shows acceptable values of the standard deviation (less than 4%) and the correlation coefficient (over 0.92). The plots in **Figure 3** can be used directly for calibrating the LIDAR maps, shown above, in mass concentration.

2.3 LIDAR images of PM fields along the sounding directions

The city of Sofia is located in a valley surrounded by several mountains, which determine the meteorological conditions characterized by reduced possibility of self-cleaning of the atmosphere. Near-ground temperature inversions occur very often in the winter-spring transition period, on windless days, and in a stable atmosphere, with negative ecological effects due to the retention layer formed leading to increased concentration of pollutants in the boundary ground layer. The weather particularities motivated our choice of period of experimental observations, namely, February-March 2018 and 2019.

The object of our studies was the air pollution on windless days at two typical urban area points. (i) Intensive traffic (IT)—Tsarigradsko Chaussee Blvd. is the busiest thoroughfare in Sofia city with grade-separated dual carriageway in almost its entire length of 11.4 km, running from the northwest to the southeast.
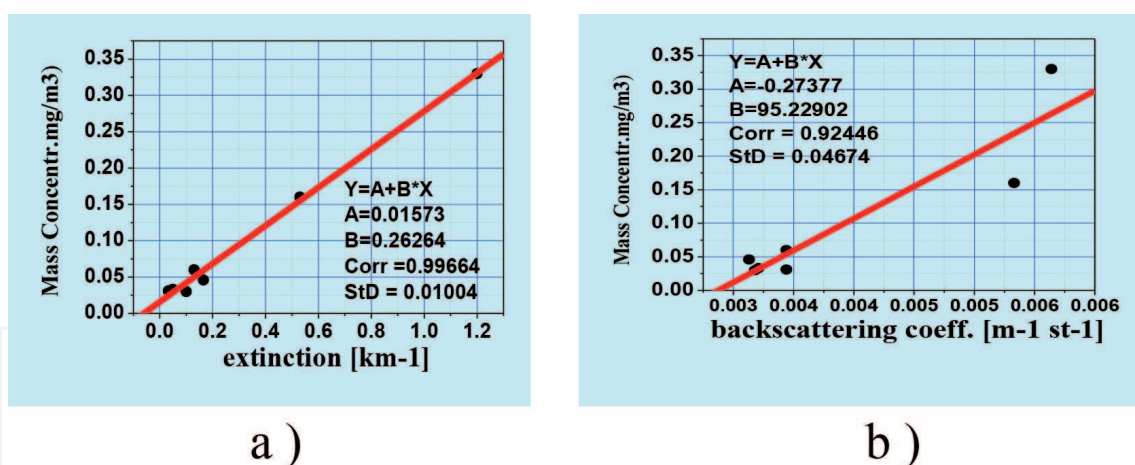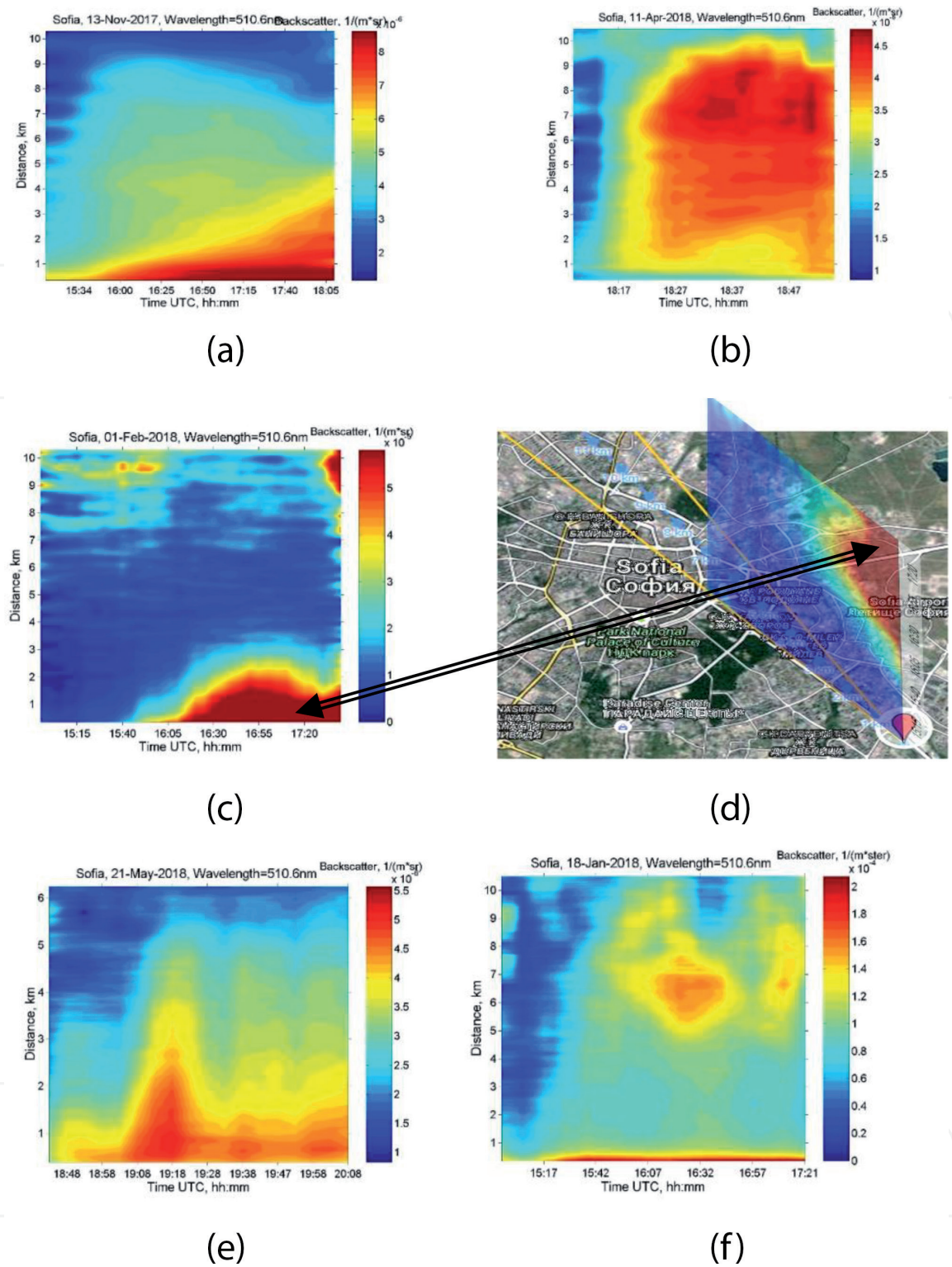
Figure 3.
Calibration plots for direct calculation of the aerosol mass concentration by both the extinction (a) and backscattering (b) coefficients.

The average intensity of the traffic according to Sofia Municipality is about 6000 vehicles per hour (Sofia Municipality Report 01.10.2017). The second sampling point was located at (ii) green area (GA) which was chosen at about 6.5 km (600 m ASL) from the LIDAR station on the roof of the Faculty of Biology of St. Kl. Ohridski University of Sofia; the building is located at a relatively busy thoroughfare, which forms a borderline between a green residential area and the largest city park.

Our LIDAR observation schedule complied with the generally accepted manner of measuring the aerosol mass concentration by air-quality monitoring systems. The sampling device pumps atmospheric air through the filter (typically a volume of 60–100 m^3) for an interval of about a few hours. Thus, the laser beam was stationary and directed to pass above the aspirator at a height of $h_{PM} < \delta R$, $\delta R \sim 30$ m being the LIDAR's radial resolution (point 1, **Figure 1**). The height of placing the aspirator was also chosen to comply with this condition, $h_{asp} < \delta R$. We thus could assume that we could neglect the vertical inhomogeneities of the atmospheric density. The LIDAR signals represent the number of backscattered photons $L_{phot}(k\delta R, \tau_m)$, where $k = 1..K_{max}$, $K_{max} = R_{max}/\delta R$, and $\tau_m = 5$ min are the time interval of photon accumulation. The total time of measurement lasted from 1 to several hours, depending on the particular weather situation. The computer system processes the input data by solving the LIDAR Eq. (1), with its output being profiles of the backscatter coefficient $\beta(k\delta R)$ or the extinction coefficient $\varepsilon(k\delta R)$, as calibrated in terms of aerosol mass concentration (see **Figure 3**). The set of LIDAR profiles obtained for the entire period of measurement is used to construct 3D LIDAR maps, with the x axis presenting the accumulation time with a step of $\tau_m = 5$ min and the y axis the distance from the LIDAR with a step δR. The z axis corresponds to the color-coded coefficients of backscatter or extinction. Thus, the position of the LIDAR station on the map has coordinates (0,0) at the start of measurements.

The series of figures below presents a set of such 3D LIDAR maps illustrating the aerosol loading space-time distribution within the region of LIDAR sounding and the aerosol sampler disposition. **Figure 4a** and **b** is a 3D LIDAR map of the backscatter coefficient distribution $\beta(k.\delta R, j.\tau_m)$, $k = 1..K_{max}$, and $j = 1..J_{max}$; the vertical axis presents the distance to the LIDAR station with a step of $\delta R = 30$ m and $K_{max}.\delta R > 10$ km, and the horizontal axis is the time (UTC) elapsed since the LIDAR sounding start (step of $\tau_m = 5$ min). **Figure 4a** and **b** is 3D LIDAR maps of the backscatter coefficient distribution $\beta(k.\delta R, j.\tau_m)$, $k = 1..K_{max}$, and $j = 1..J_{max}$; the vertical axis presents the distance to the LIDAR station with a step of $\delta R = 30$ m and $K_{max}.\delta R > 10$ km, and the horizontal axis is the time (UTC) elapsed since the LIDAR sounding starts (step of $\tau_m = 5$ min). The duration of sounding $\tau_{prob} = J_{max}.\tau_m$ exceeded 3 h.

(a)

(b)

(c)

(d)

(e)

(f)

Figure 4.
(a and b) Hourly aerosol pollution loading (as 3D LIDAR maps) over the urban area with intensive traffic. LIDAR image (c) is overlapped in vertical position on the Google Maps (d) of the Sofia central part. Position of the LIDAR station is well seen. Such presentation is useful for simultaneous space-time tracing of the strong PM formation over the monitored area. (e) and (f) 3D LIDAR maps, demonstrating cases of complicated space-time dynamics of aerosol fields, transporting bioaerosol, emitted mainly by different local regions of the large city.

The backscatter coefficient $\beta(k.\delta R, j.\tau_m)$ is color-coded in terms of mass concentration, with the dark brown areas corresponding to the zones of the highest PM concentration and the light blue ones, to the lowest PM concentration. As seen, this approach allowed to follow the temporal behavior of the PM aerosol loading along the LIDAR sounding path to a distance of more than 10 km. For example, **Figure 4a** demonstrates that in the early afternoon hours, where the automobile traffic is relatively light, the aerosol loading is low, especially in the zones away from the downtown area. As

the working day is nearing its end, the traffic intensity rises, and, correspondingly, the LIDAR response shows increasing mass concentration along the boulevard. The distances near the LIDAR station are characterized by very high mass concentration, since the LIDAR station (IE-BAS) is located close to the busy road junction—Tsarigradsko Chaussee Blvd. crossing with another four-lane boulevard. The image in **Figure 4b** illustrates the passing of a larger aerosol formation of length to the order of 8 km along the boulevard. In such cases we typically founded heavy bioaerosol loadings, emitted by the near disposed populated regions of limited areas of order of 1–2 km^2.

The images in **Figure 4c** illustrate a relatively small aerosol formation (as in **Figure 4b**), passing near the LIDAR station. The same image can be overlapped (in vertical disposition) on the Google Maps of the Sofia central part (**Figure 4c**) for better identification of the disposition of the emitted aerosol formation.

We should emphasize here the important point that the LIDAR maps can be used to follow the bioaerosol transport and to estimate the probable location of their sources. One could also draw the conclusion that, when the methodology discussed is employed, the sampling device location is not so critical in what concerns observing microorganisms in the air and establishing the contamination sources. The incorporation of the proposed LIDAR-based methodology into the city monitoring system could provide many additional advantages, such as forecasting the effects of selected bioaerosol loadings on the entire large city area, e.g., using modeling algorithms. The successful scanning by the LIDAR system in different directions (see **Figure 1**) could provide additional information for improving the local authorities' decision-making process.

2.4 Sampling and analytical methods

In the experiments presented, we directed the LIDAR beam to intense traffic area and green area to probe the near-surface atmosphere in a constant horizontal direction. The measurement time covered practically the entire period of the late afternoon traffic maximums, while maximums of the PM pollutions were clearly observed in the backscattered LIDAR signals, as received and processed by our system. The samples were taken in situ using a Hygitest 106 (Maimex), a high-efficiency portable device for sampling and concentration determination of PM in atmospheric aerosol. The apparatus allows simultaneously to take samples at four canals with a possibility to regulate the volume of air passing through the filters. The flow-rate of the aspirated air was measured by the sampling unit. The sampled volume was chosen to be smaller than the LIDAR resolution volume (typically ~250–300 m^3).

The dust was collected on a filter (borosilicon oxide) with #3 μm and #8 μm (FILTER-LAB, Material MCE, Lot.180509006 and 07). Also analytical filters #0.2 μm type FPP-15-2568-411-05795731-2008 were used, consisting of a layer of ultrathin threads (diameter of 1.5 μm) deposited on a piece of fabric and designed to collect aerosol particles of size exceeding 0.2 μm. Additionally, the material collected in situ on the filters after 3 h of aspiration during the LIDAR monitoring was studied by a number of methods: metal analysis (MA) has been carried out by devices and equipment—ICP-OES, PlasmaQuant PQ 9000 Elite (Analytik Jena), sample visualization, and PM morphological by scanning electron microscopy (SEM) and energy-dispersive and X-ray fluorescence systems (EDAX). Chemical composition, phase analysis, and particle size distribution were made using powder X-ray diffraction (XRD), photoelectron spectroscopy (XPS), and infrared (IR) spectroscopy. Phase identification was performed with the X-Pert program using ICDD-PDF2. Important tools for structural measurement was Mössbauer analysis which was made using apparatus Wissenschaftliche Elektronik GmbH, working with a constant acceleration mode: 57Co/Cr source, α-Fe standard. The sampling

for investigation of microbiota in bioaerosols formed was achieved using a Hygitest 106 and axa replica technique on nutrient agar as well as Koch sedimentation method. Different elective media as nutrient agar; nutrient media for oligotrophs, actinomycetes, and fungi; blood agar; phenylethyl alcohol agar; MacConkey agar; and bacteria mobility-test medium [17] were used. Culturable bacteria isolated as pure cultures were identified by the methods of classical taxonomy [18] and the methods of the molecular taxonomy based on the PCR of 16S rDNA with universal eubacterial primers [20]. Molecular identification of the fungal strains was performed by PCR of the rDNA internal transcribed spacers (ITS) and primers ITS1 and ITS4 [21]. Positive PCR products were purified and sequenced (Macrogen Inc. Amsterdam, The Netherlands).

3. Particulate matter characterization

The natural aerosols are mixture of PM with highly varied crystallo-chemical structure bioaerosols, which are mixture from fungal spores, pollen, plant, etc. The particle research evaluation is a need for integrating the development of continuous monitoring technologies for determining both particle mass and chemical, physical, and biological methods for their identification. Such studies are of importance in determining the health and welfare effects of urban pollution and city transportation planning. As illustrated by **Figure 4**, we proved the possibility of a fast detailed remote analysis and monitoring of the air pollution over large urban regions, providing fast estimates of the air pollution transport over the city, as well as determination of pollution source location. Once a place of high PM concentration was localized by the LIDAR, samples were taken as described above. Initially, the particles were immobilized on single or multiple filters. This was followed by covering with a conductive carbon film deposited by sputtering of spectroscopically pure carbon in high vacuum. The experimental procedure allows for observing the particles' morphology and determining their mean size (**Figure 5a** and **b**) by means of SEM, EDAX, and MA.

The SEM images of the material collected on the filters after 3 h of aspiration during the LIDAR monitoring showed a large amount of particles larger than 2.5 μm and some amount of small particles (under 2.5 μm); most of the particles are included in quasi-aggregated structures, where nanosized particles could also be seen. **Figure 5a** illustrates the wide variety of quasi-spherical particles with an

(a)   **(b)**
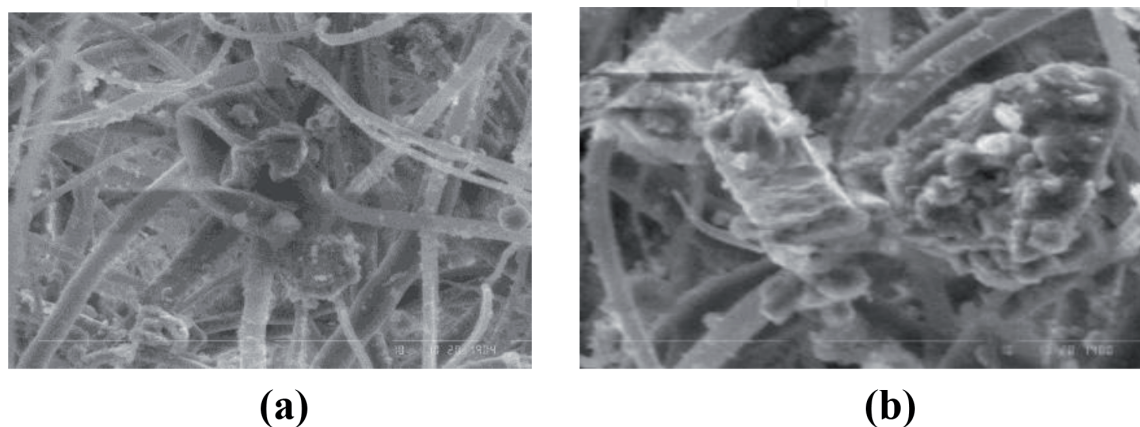
Figure 5.
SEM images of the particles under different magnification; the fibers reveal the filter structure of (a) PM with size ≥ 3 μm and (b) PM with size between 0.2 and 3 μm.

average size of about 2.5 μm. **Figure 5b** shows a typical shape of PM particles with sizes between 2.5 and 10 μm, which are agglomerates of hybrid origin.

3.1 Particulate matter distribution and metal's concentration analysis

Diameters of the PM varied from 20 nm to a more than 10 μm for pollen or plant debris [22–24]. After selecting typical particle images based on 10 points on the filter's surface, the percentage distribution of the particles with different sizes was obtained. The particles' size distribution study was conducted following the technique of random lines crossing particles of various diameters on optical microscopy and SEM images of immobilized PM particles under different magnification.

The SEM images of the material collected on the filters after 3 h of aspiration during the LIDAR monitoring showed a large amount of particles. The airborne PM can be divided into three classes (**Figure 6**), fine PM particles 2.5 μm in diameter or smaller, coarse PM particles 2.5–10 μm in diameter, and PM ≥ 10 μm, which differ not only in size but also in source, chemical composition, physical properties, and formation process. Major sources of $PM_{2.5}$ could be produced by motor vehicles, residential fireplace fossil fuel combustion by industry and wood stoves, vegetation burning, and smelting or other processes [25]. Our investigation for the period of 2 years showed that in the intensive traffic area, the majority of the particles are smaller than 10 μm as produced by automobile exhaust emissions, while in the green area, bigger particles appeared most probably from the wooded zone.

The studies conducted during the winter-spring transition period of 2018 and 2019 highlighted the alarming trend of increased content of the Cu, Fe, and Zn metals over the permissible concentration values [25]. **Figure 7** presents summarized data for two of the locations (blue is limited value, red dot is intensive traffic, and green dot is green area) that were objects of our studies considered here.

The above results were confirmed by EDAX measurements of PM collected by the functional filters. **Figures 8** and **9** demonstrate the presence of Cu and Fe. Less frequently, the presence of Pb was also noticed, again exceeding the permissible concentration values (**Figure 8**).

3.2 Crystallo-chemical structure of PM

Great attention in the physicochemical characterization of investigated PM samples was paid to compounds related to the observed overconcentrations of certain elements (**Figure 5**). The chemical elements are varying from main component level to trace elements. **Figure 10** shows the representative powder X-ray diffraction
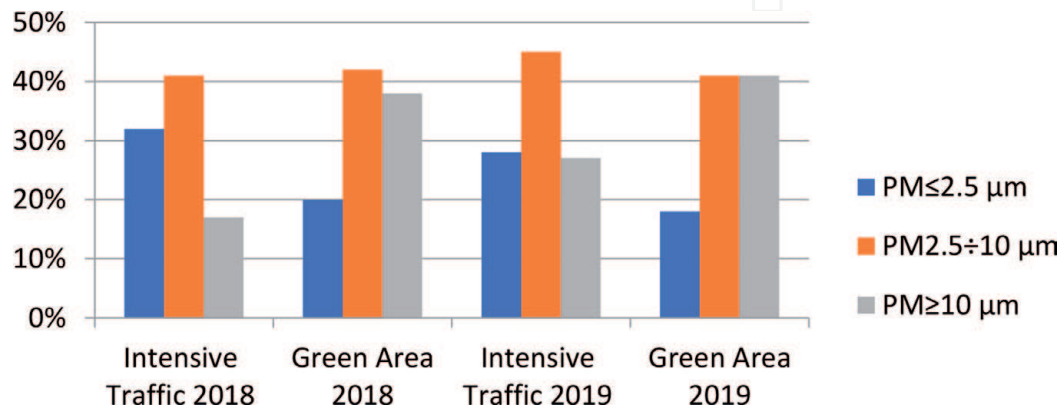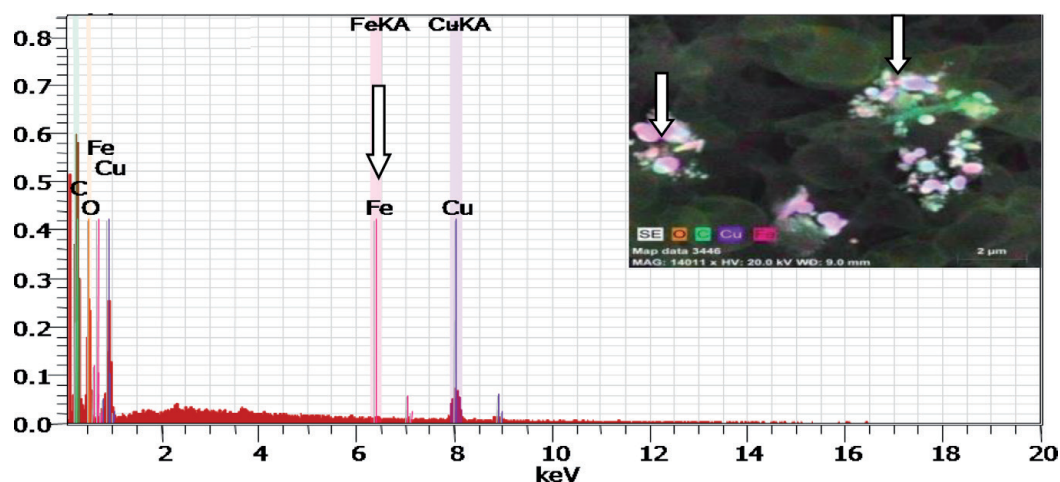

Figure 6.
Particle size distribution in two points in the urban area of Sofia City (for period of investigation February–April 2018 and 2019).
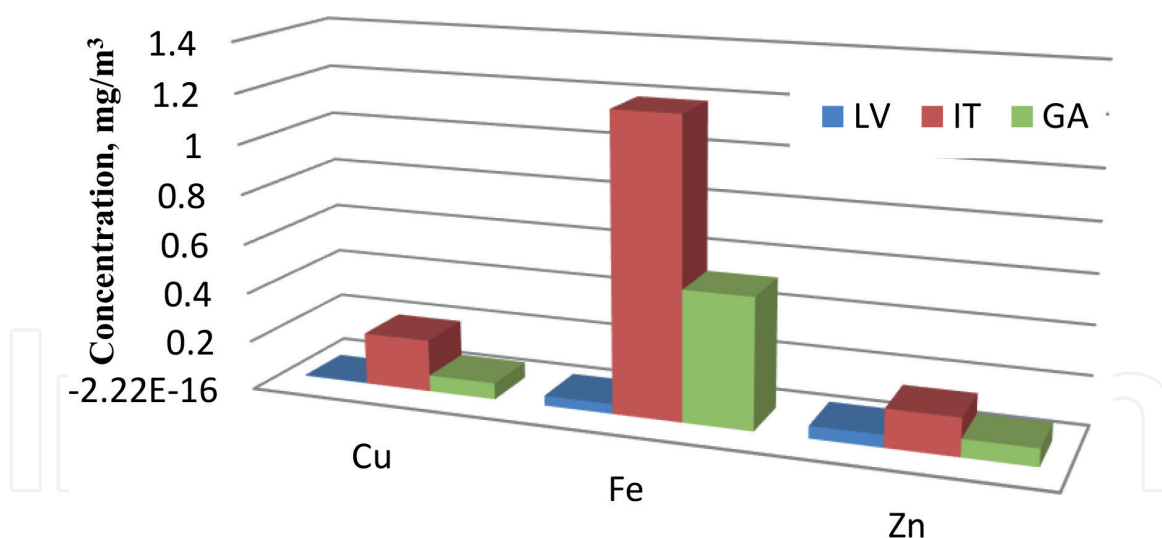
Figure 7.
Metals with concentrations exceeding the permissible limiting values (LV); the blue bars indicate the LV (annual average of mg/m³), and red and green bars indicate the average concentrations in an intensive traffic (IT) and a green area (GA), respectively, as estimated by our LIDAR measurements.
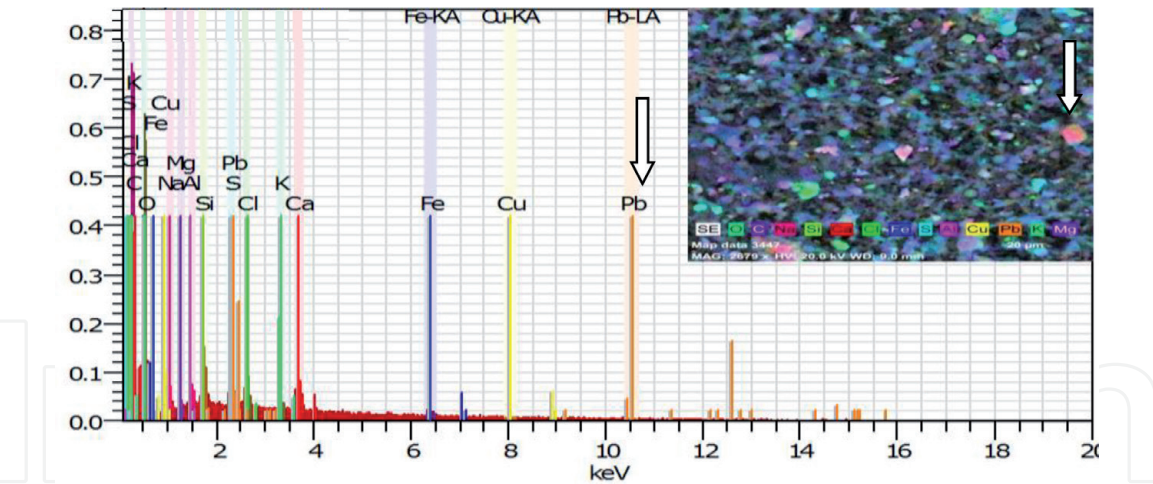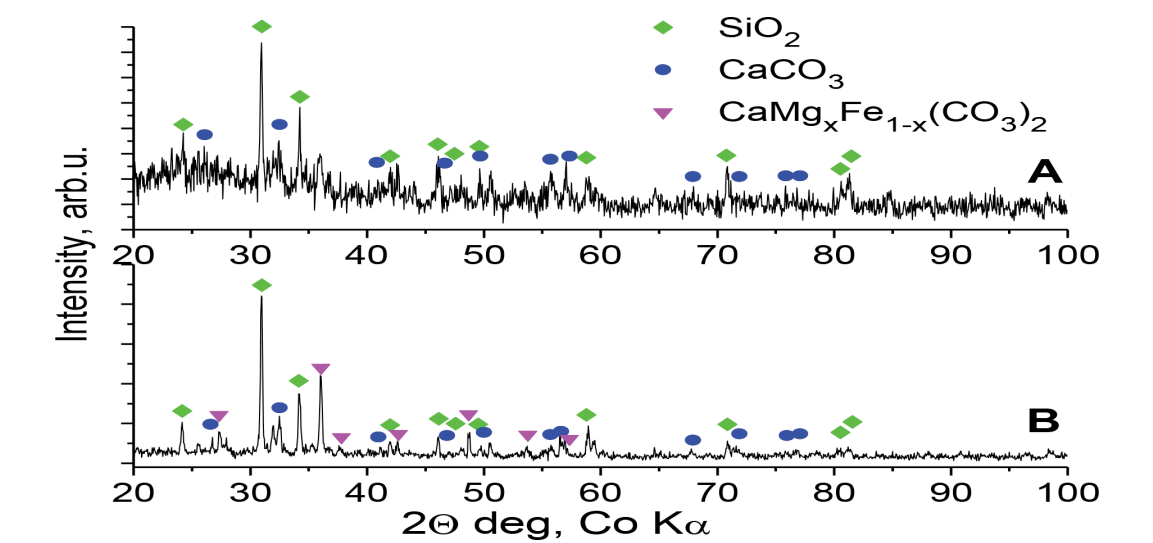

Figure 8.
EDS spectrum of element analysis and the insert presents SEM image of the element's distribution on the fixed particle adsorbed on the filters from IT zone (23.03.2019).

patterns of studied PM samples originated from different areas (IT and GA). The existence of low intensity and broad X-ray diffraction peaks laid on nonselective background in all registered patterns was observed. The main crystallite phases detected in X-ray diffractograms are silicates and aluminosilicates and carbonates. Lesser amounts of different sulfates were found also. Registered X-ray amorphous halos and nonselective background together with small intensity and high width of diffraction peaks of all registered crystallite phases indicate nearly amorphous structure, small particle size, and low crystallinity degree of PM material from both studied locations. The observations are in good consideration with obtained elemental composition and SEM analysis of studied materials. Regarding both analyses it could be concluded that PM greatly vary in size from nanometers to several tenths of micrometers. However, most of the particles on SEM images are aggregates of smaller particles (**Figure 8**).

Based on the obtained big iron content in studied PM, ^{57}Fe Mössbauer spectroscopy was applied to investigate samples. It allows to go deeper into the PM characteristics and to make more clear conclusions about the presented iron-bearing chemical compounds, their quantity, and dispersion. Represented
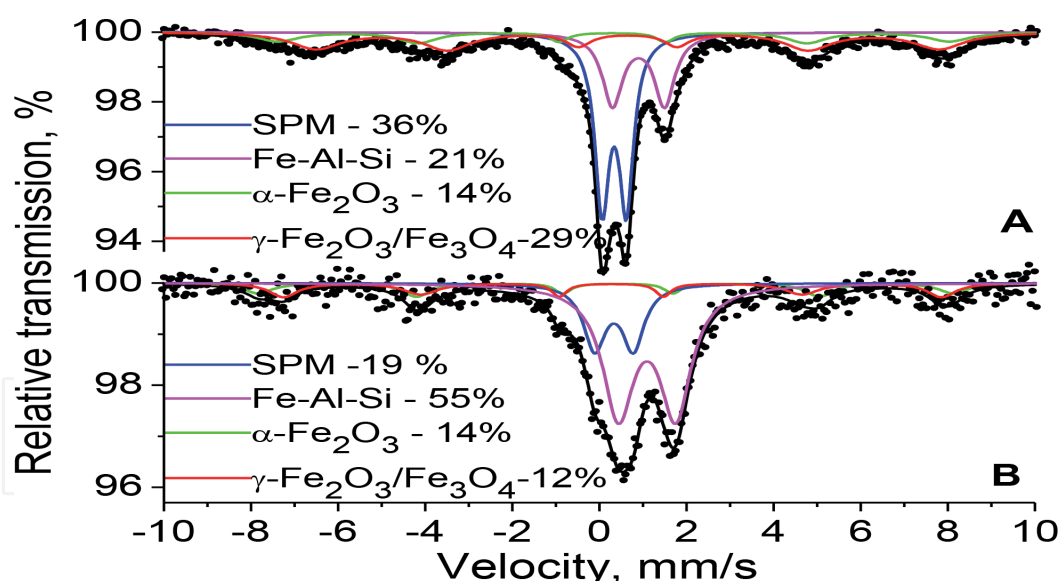
Figure 9.
EDS spectrum of element analysis and the insert presents SEM image of the element's distribution on the fixed particle adsorbed on the filters from IT zone (23.03.2019).

Figure 10.
Representative X-ray diffraction patterns of studied powder PM originated from IT (A) and GA (B).

Mössbauer spectra of samples can be seen on **Figure 11**. Sextet and doublet components were obtained after spectrum evaluation. They have the characteristic parameters of phases presented on the respective figures (**Figure 11A** and **B**). The main differences between studied PM from IT and GA could be regarded to quantity of presented phases and their particle size. After spectrum evaluation the sextet components with hyperfine parameters characteristic for spinel phase were resolved, highly non-stoichiometric magnetite $Fe_{3-x}O_4$ phase (or maghemite phase γ-Fe_2O_3) in all studied samples. Their quantity is much bigger in high-traffic area than in residence green area (29% vs. 12%). On the other hand, the calculated values of hyperfine effective fields of all registered magnetic phases (both spinel and hematite phase) are lower than the typical ones for the respective bulk phases. So it can be concluded that the particle size of these oxide phases is lower than 20 nm [26, 27]. Hematite phase dispersion is almost the same in IT and GA samples, but maghemite/magnetite phase particle size is smaller in IT area. It can be well seen on **Figure 11** that the doublet components are the main part of all PM spectra. According to the calculated hyperfine parameters of these doublets and comparison with previous investigations, it can be concluded that the majority of Fe-bearing compounds in IT PM are superparamagnetic (SPM) phases with nanometric size

Figure 11.
Representative Mössbauer spectra of studied powder PM originated from IT (A) and GA (B)

(oxides or hydroxides). Fe^{3+} in paramagnetic phases as glass phases, sulfates, clay minerals, etc. is also presented in both locations (also in this component) [28]. Fe^{2+} was found in paramagnetic component indicative for the presence of aluminosilicate glass, ankerite, iron-containing carbonates or clay minerals, etc. [29]. The last component is the largest component in GA Möessbauer spectrum (see **Figure 11B**).

Comparative analysis of registered FTIR spectra of PM reveals appearance and increasing of bands typical for the organic compounds and inorganic salts (mainly sulfates and phosphates) typically presented on the surface of studied particles [30]. Obtained results indicate that silicates contributed to the highest percentage of total analyzed IR spectra signal for particles at both locations. Organic compounds are hydrocarbons and substituted hydrocarbons, adsorbed CO, etc. They could be regarded to partially oxidized products of fuel combustion. Registered X-ray photoelectron spectra of samples gave additional information for presented surface elements and their concentrations and chemical state. C, O, Si, Al, Ca, N, Na, and S have been detected on the PM surface. The determined binding energies are typical for Si-O, Al-Si-O, Ca-CO$_3$, C-H-N, C-H-NOx, C-H-N-Cl, Na-C-H-N-Cl, Cu-Cl-C-N-H-O, and Cu-O bonding, respectively [31]. Trace levels of Fe, Cu, Zn, and Cl were also found, and this could be related to automobile exhaust emissions and to brakes and tire wear. So, the analysis shows that the surface of investigated PM sample consists mainly of silicate and aluminosilicate compounds, as well as of different organic and inorganic carbon phases/carbonaceous species. XPS showed the presence of carbon black, which was attributed to the oxidative wear and subsequent deposition from related volatiles, as well as of graphitic particles emitted as a result of abrasive wear. The last one was registered in XRD patterns also. According to the literature data, most of the surface carbon comes from burning of fossil fuels, which is not surprising as all the samples were collected in winter period [32].

The analysis of obtained results using different characterization methods—XRD, Mössbauer, IR, and XPS—allows us to make conclusions about chemical composition of studied airborne PM, as well as about the quantity, crystallinity degree, and dispersion of compounds. The main phases registered in samples from both IT and GA are silicate, aluminosilicate, clay minerals, and sulfate compounds, as well as organic and inorganic (carbonate and coal) carbon phases. Elemental analysis showed that the Fe is the dominated metallic content in high-traffic area. The obtained bigger than usual content of iron in PM could be regarded to the

airborne particles produced by transport and mainly by car engine performance [33]. This also explained the observation of higher iron content in IT samples compared to those from GA. On the other hand, Fe, Cu, Zn, Pb, and S in relatively high concentrations in all measured airborne PM (see **Figure 7**) could be regarded to abrasion of car brake lining material. Although the Pb is having been replaced in modern brake linings, the presence of cars older than 15–20 years is probably the explanation of registered Pb content in studied PM. This is an important issue for further regulations. Smaller quantity of other metals as Ba, Mg, Ni, and K has been found, which also could be considered as a result of car lining wear. Fe domination among trace elements was attributed to the easiest fragmentation of Cu, Zn, and Sn due to their lower mechanical properties, as well as their lower melting points, compared to steel and cast iron. Therefore, car braking could be considered to be one of the major sources of nonexhaust traffic-related emissions in all urban locations. The main source of silicate and aluminosilicate compounds could be considered to be mostly natural (silicate, aluminosilicate, clay minerals). The anthropogenic factors in PM formation are connected with street and house reparation activities. The noticeable concentrations of organic substances and elemental carbon have been recognized as a result of incomplete fuel combustion, lubricant volatilization during the combustion procedure, and residuals from the exhaust gases originating from power plants, small houses and different engines, road surface wear, etc. [34–37].

3.3 Bioaerosols

Bioaerosols may contain pollen, bacteria, actinomycetes, fungal spores, and sneezing and cough drops, as well as endotoxins, mycotoxins, and allergens. A number of studies have shown that bacteria in the air most commonly coexist with particulate matter and are thus transported over long distances [38, 39]. The average residence time of bioaerosols in the atmosphere may be from day to several weeks, depending on their size and aerodynamic properties [40]. Larger bioaerosol particles are retained in the upper airways of the human (oral and nasal cavities), while smaller ones can reach the lower pathways in the lungs [41, 42]. They can have a different negative effect on humans (infectious diseases, toxic effects, allergies, and even cancers). Most commonly, the symptoms and diseases resulting from the inhalation of bioaerosols are related to the respiratory system. Causes of some human infections, such as measles or tuberculosis, can spread through bioaerosols containing infectious microorganisms [43, 44]. Fungal spores, as part of bioaerosol particles, are most often associated with asthmatic symptoms and are a risk factor for various respiratory problems. Pulmonary plague caused by *Yersinia pestis* can spread after inhalation of bioaerosol particles containing the pathogen. Qualitative and quantitative composition of microorganisms varies greatly [2]. In the air over Erdemli, Turkey, during the passage of Saharan dust in March 2002, bacteria belonging to seven genera were isolated, and the majority of the species were referred to the genus *Streptomyces* [45]. In Bamako, Mali, representatives of 20 genera were identified during the passage of a large amount of desert dust, with *Bacillus* species representing 38% of all isolates, followed by genera *Kocuria* (12.8%), *Saccharococcus* (7.4%), and *Micrococcus* (6.4%). From the 95 species of bacteria identified in this study, about 10% are potential pathogens in animals, 5% are phytopathogens, and 25% are opportunistic human pathogens [46].

Eukaryotic microorganisms from genera *Cladosporium*, *Alternaria*, and *Epicoccum* are the dominant species found in open air in different parts of the world, while species of the genera *Penicillium* and *Aspergillus* are more often isolated from enclosed spaces [47]. Saharan sandstorms are responsible for the

transmission of pathogens associated with widespread coral infections (predominantly *Aspergillus* genus) in the Caribbean region [48–50].

The concentration of bioaerosol particles varies greatly depending on the weather, location, and annual seasons. The wind, rain, solar radiation, and ozone are factors that influence the concentration of microorganisms in the air and may even have a bactericidal effect. The survival of bacteria in the air decreases with increasing temperatures as it begins to decrease when temperatures exceed 24°C [44–52]. High relative humidity (RH) can significantly reduce the bactericidal effect of ultraviolet light and hence increase the survival of bacteria [53]. Quantitative composition also influences some pollutants in the air, for example, formaldehyde, acrolein, ozone, and sulfur dioxide, which have a negative effect on the viability of the bacteria [54]. Due to the strong influence of these factors, the quantitative composition of the air microbiota is unstable and depends on local sources of pollution. Statistics based on the results of the US Environmental Protection Agency study show that bacterial concentration in open spaces is higher than in indoor pools [55]. The average concentration of all bacteria isolated from outdoor air is 10^2 CFU/m^3. Ninety-five percent of the culturable bacteria are mesophilic. In a study conducted in the United States, it has been found that the concentration of fungi is usually higher in open spaces than in the indoor. The highest concentration of fungi is measured in autumn and summer and the lowest in winter and spring. In open spaces, the concentration of fungi varies strongly from 1 to 8200 CFU/m^3 of air, with an average count of about 540 CFU/m^3 [56].

Fungi and their spores are more resistant to stress in the air environment than viruses and vegetative cells of the bacteria [44, 52]. Higher temperatures, wet substrates, and humidity provide favorable conditions for fungal development [57]. The quantitative analysis of the microbiome of air bioaerosols in the points tested reviled the presence of aerobic heterotrophic and oligotrophic microorganisms and fungi (**Tables 1** and **2**).

The analysis of the results obtained show that the quantities of the heterotrophic and oligotrophic microorganisms in the air of the first location mentioned are significantly higher. It is also obvious that the levels of these microorganisms in both points had a tendency to decrease during warm summer period, which correlated with lower urban traffic at this period. It must be noted that the quantity of fungi in the second location is significantly higher than the detected levels in the first one, but there is a tendency to increase during spring-summer period. The results are similar to those found by other authors [45, 46, 58–60]. Fifty-six pure cultures isolated from both points tested subjected to taxonomic investigation. More than 45% of the isolates are Gram-positive and belong to genus *Bacillus* (*B. cereus*, *B. pumilus*, *B. subtilis*, *B. megaterium*, *B. thuringiensis*, and *B. mycoides* are the dominant species). Information about the prevalence of such bacteria in similar sampling locations is available in the literature [39, 58, 60, 61].

Microorganisms	Quantity of the detected microorganisms CFU/m^3			
	Sampling January	Sampling May	Sampling August	Sampling November
Heterotrophic MO	64,256 ± 2.1	36,343 ± 2.4	32,147 ± 3.1	50,382 ± 1.5
Oligotrophic MO	56,950 ± 2.5	29,412 ± 1.8	27,876 ± 1.1	52,356 ± 2.3
Fungi	3747 ± 1.1	5223 ± 2.1	5322 ± 1.7	3245 ± 1.2

Table 1.
Quantitative analysis of culturable microorganisms in the air of the intense traffic.

Microorganisms	Quantity of detected microorganisms CFU/m^3			
	Sampling January	Sampling May	Sampling August	Sampling November
Heterotrophic MO	9741 ± 1.1	6182 ± 2.1	5932 ± 1.8	83,462 ± 1.3
Oligotrophic MO	9086 ± 1.9	4777 ± 1.1	5323 ± 2.2	10,321 ± 2.1
Fungi	2248 ± 1.7	8992 ± 1.3	6332 ± 0.9	4672 ± 1.1

Table 2.
Quantitative analysis of culturable microorganisms in the air of the point green area.

The molecular analysis and sequencing confirmed these results. *Erwinia herbicola* was the dominant species from family *Enterobacteriaceae*. *Bacillus megaterium* and *Bacillus pumilus* as well as *Rathayibacter caricis*, *Arthrobacter* sp. *FXJ8.160*, *Acidovorax* sp. *NA2*, *Plantibacter flavus*, and *Kocuria rosea* were most frequently isolated. It can be summarized that from the group of Gram-positive bacteria in both locations, 48% of the isolates were related to *Bacillus* genus; 21% of all isolates were related to the *Enterobacteriaceae* family; 10% were related to the *Arthrobacter* genus; 4% were related to the genus *Exiguobacteria*; and 2% of the isolated microorganisms were related to the genera *Staphylococcus*, *Acidovorax*, *Plantibacter*, *Gordonia*, *Streptomyces*, *Kocuria*, and *Rathayibacter*. It is noteworthy that contingent pathogens (*Bacillus cereus*, *Bacillus pumilus*, *Erwinia herbicola*, *Enterobacter aerogenes*) are found among the isolates and such pathogens are also found in other studies of airborne microbial load [45]. Representatives of the genus *Gordonia* are conditionally pathogenic and isolated from sick patients. Representatives of the genus *Kocuria* are part of the resident microflora of the skin and mouth in humans but are also widespread in all elements of the environment. Representatives of the genus *Rathayibacter* cause serious damage to the nervous system.

Fungal isolates from both points investigated belong mainly to genera *Aspergillus* (*Aspergillus fumigatus*, *Aspergillus versicolor*), *Penicillium* (*P. sanguifluum*, *P. chrysogenum*, *P. brevicompactum*), *Cladosporium* (*C. sphaerospermum*), *Botrytis* (*B. cinerea*), and *Symmetrospora*. Some of these fungi isolated are typical human pathogens [47–49]. All these findings confirmed the idea that the investigations on particular matters (PM) must combine obligatory with analyzing of the microbiota in air aerosols.

4. Conclusions

The LIDAR monitoring methodology discussed opens up possibilities for rapid space-time identification and characterization of physicochemical and bio-pollution processes over the entire territory of large cities without affecting the normal living patterns of the city residents. Remote sensing allows one to locate the occurrence of pollution, which can be easily combined with in situ sampling. The experimental results described above clearly showed that at points of extreme pollution, the small-size particles (less than 2.5 μm) predominated in areas of heavy traffic, while nanosized PM were also found. Further, in intensive traffic areas, we observed metal particles, whose concentrations exceeded the maximal admissible levels. LIDAR sounding of "greener" areas revealed the predominant presence of particles with sizes ≥10 μm; the analyses conducted indicated their prevailing biological origin. The LIDAR maps created can be further used for tracing the full air-mass transport, carrying contamination from a number of pollution sources

(chemical, biological, dust, etc.) distributed over the scanned region. Finally, we should emphasize the simplicity of the LIDAR and the aerosol sampling equipment used and, thus, the possibilities for its wide use in any populated region, where keeping the air quality within tolerable levels is problematic. We should once again note that methodology developed affects negligibly the residents' lifestyle in urban regions. Therefore, it is our belief that it offers promising paths for wide application in air-quality monitoring in highly polluted large urban areas.

Acknowledgements

Author details

Dimitar Stoyanov[1], Ivan Nedkov[1]*, Veneta Groudeva[2], Zara Cherkezova-Zheleva[3], Ivan Grigorov[1], Georgy Kolarov[1], Mihail Iliev[2], Ralitsa Ilieva[2], Daniela Paneva[2] and Chavdar Ghelev[1]

1 Institute of Electronics, Bulgarian Academy of Sciences, Sofia, Bulgaria

2 Faculty of Biology, St. Kliment Ohridski University of Sofia, Sofia, Bulgaria

3 Institute of Catalysis, Bulgarian Academy of Sciences, Sofia, Bulgaria

*Address all correspondence to: nedkovivan@yahoo.co.uk

IntechOpen

References

[1] Fuzzi S, Baltensperger U, Carslaw K, Decesari S, Denier van der Gon H, Facchini MC, et al. Particulate matter, air quality and climate: Lessons learned and future needs. Atmospheric Chemistry and Physics. 2015;**15**:8217-8299. DOI: 10.5194/acp-15-8217-2015

[2] Brodie EL, De-Santis TZ, Moberg Parker JP, Zubietta IX, Piceno YM, Andersen GL. Urban aerosols harbor diverse and dynamic bacterial populations. Proceedings of the National Academy of Sciences of the United States of America. 2007;**104**(1):299-304. DOI: 10.1073/pnas.0608255104

[3] Jones AM, Harrison RM. The effects of meteorological factors on atmospheric bioaerosol concentrations—A review. Science of the Total Environment. 2004;**326**(1-3):151-180. DOI: 10.1016/j.scitotenv.2003.11.021

[4] Macher J. Bioaerosols: Assessment and Control, American Conference of Governmental Industrial Hygienists. USA: OH Cincinnati; 1999. 322 p. ISBN: 978-1-882417-29-1

[5] Stanley RG, Linskins HF. Pollen: Biology, Chemistry and Management. 1st ed. Berlin, Germany: Springer Verlag; 1974. DOI: https://www.springer.com/gp/book/9783642659072

[6] Gregory PH. The Microbiology of the Atmosphere. 2nd ed. London: Hall; 1973. 377 p. DOI: https://catalogue.nla.gov.au/Record/395639

[7] Maricovich H, editor. Black's Medical Dictionary. 42nd ed. USA: A&C Black; 2009. p. 765. ISBN-10:9780713689020

[8] Measures RM. Laser Remote Sensing: Fundamentals and Applications. 1st ed. NY, USA: Wiley&Sons; 1984. 510 p. DOI: https://www.worldcat.org/title/laser-remote-sensing-fundamentals-and-applications/oclc/123159913

[9] Kovalev VA, Eichinger WE. Elastic LIDAR: Theory, Practice, and Analysis Methods. 1st ed. NY, USA: Wiley&Sons; 2004. 615 p. DOI: 10.1002/0471643173

[10] Weitkamp C, editor. LIDAR Range-Resolved Optical Remote Sensing of the Atmosphere. Springer Series in Optical Sciences, Springer; 2005. 456 p. DOI: 10.1007/b106786

[11] Stoyanov D, Dreischuh T, Grigorov I, Kolarov G, Deleva A, Peshev Z, et al. Near surface aerosol LIDAR mapping of Sofia Area. On the synergy with city sensor network. In: Proceedings of the Final Meeting—Sixth Sci. Meeting EuNetAir. 2016. pp. 61-64. DOI: 10.5162/6 EuNetAir2016/16

[12] Simard JR, Roy G, Mathieu P, Larochelle V, McFee J, Ho J. Standoff Integrated bioaerosol Active Hyperspectral Detection (SINBAHD): Final Report. 2002: DREV-TR-2002-125. DOI: pubs.drdc-rddc.gc.ca/BASIS/pcandid/www/engpub/DDW?W%3DSYSNUM=518849

[13] Simard JR, Roy G, Mathieu P, Larochelle V, McFee J, Ho J. Standoff sensing of bioaerosols using intensified range-gated spectral analysis of laser induced fluorescence. IEEE Transactions on Geoscience and Remote Sensing. 2004;**42**(4):865-874. DOI: 10.1109/TGRS.2003.823285

[14] He TY, Stanič S, Gao F, Bergant K, Veberič D, Song Q, et al. Tracking of urban aerosols using combined LIDAR-based remote sensing and ground-based measurements. Atmospheric Measurement Techniques. 2012;**5**:891-900. DOI: 10.5194/amt-5-891-2012

[15] Peshev ZY, Dreischuh TN, Toncheva EN, Stoyanov DV. Two-wavelength

LIDAR characterization of atmospheric aerosol fields at low altitudes over heterogeneous terrain. Journal of Applied Remote Sensing. 2012;**6**(1):063581. DOI: 10.1117/1. JRS.6.063581

[16] Klett J. Stable analytical inversion solution for processing LIDAR returns. Applied Optics. 1981;**20**(1):211-220. DOI: 10.1364/AO.20.000211

[17] Atlas KM. Handbook of Microbiological Media. 4th ed. Washington DC: ASM Press and Roca Raton, London, New York, USA: CRC Press; 2010. 2040 p. ISBN-10: 9781439804063

[18] Whitman W, editor. Bergey's Manual of Systematics of Archaea and Bacteria (BMSAB). Bergey's Manual Trust Publ; 2015. 2011 p. ISBN:9781118960608. DOI: 10.1002/978111896060

[19] Fernald F. Analysis of atmospheric LIDAR observations: Some comments. Applied Optics. 1984;**23**(5):652-653. DOI: 10.1364/AO.23.000652

[20] Wilson KH, Blitchington RB, Greene RC. Amplification of bacterial 16S ribosomal DNA with polymerase chain reaction. Journal of Clinical Microbiology. 1990;**28**(9):1942-1946. DOI: jcm.asm.org/content/28/9/1942

[21] White TJ, Bruns T, Lee S, Taylor JW. Amplification and direct sequencing of fungal ribosomal RNA genes for phylogenetics. In: Innis MA, Gelfand DH, Sninsky JJ, White TJ, editors. PCR Protocols: A Guide to Methods and Applications. New York.: Academic Press, Inc.; 1990. pp. 315-322. DOI: 10.1016/0307-4412(91)90165-5

[22] Fröhlich-Nowoisky DAP, Després VR, Pöschl U. High diversity of fungi in air particulate matter. Proceedings of the National Academy of Sciences of the United States of America. 2009;**106**(1):12814-12819. DOI: 10.1073/pnas.0811003106

[23] Jaenicke R. Abundance of cellular material and proteins in the atmosphere. Science. 2005;**308**(5718):73. DOI: 10.1126/science.1106335

[24] Hind WC. Aerosol Technology: Properties, Behavior, and Measurement of Airborne Particles. 2nd ed. NY: John Wiley&Sons; 2012. 504 p. ISBN: 978-1-118-59197-0

[25] World Health Organization (WHO). Health Effects of Particulate Matter. Copenhagen: Regional office for Europe; 2013. ISBN: 978 92 890 0001 7

[26] Fock J, Hansen MF, Frandsen C, Mørup S. On the interpretation of Mössbauer spectra of magnetic nanoparticles. Journal of Magnetism and Magnetic Materials. 2018;**445**:11-21

[27] De Grave E, Van Alboom A. Evaluation of ferrous and ferric Mössbauer fractions. Physics and Chemistry of Minerals. 1991;**18**:337-342. DOI: 10.1007/BF00200191

[28] Mahieu B, Ladrière J, Desaedeleer G. Mössbauer spectroscopy of airborne particulate matter. Journal de Physique Colloques. 1976;**37**(C6):C6-837-C6-840. DOI: 10.1051/jphyscol:19766176

[29] Gietl J, Lawrence R, Thorpe A, Harrison R. Identification of brake wear particles and derivation of a quantitative tracer for brake dust at a major road. Atmospheric Environment. 2010;**44**:141-146. DOI: 10.1016/j. atmosenv.10.016

[30] Ji Z, Dai R, Zhang Z. Characterization of fine particulate matter in ambient air by combining TEM and multiple spectroscopic techniques—NMR, FTIR and Raman spectroscopy. Environmental Science: Processes & Impacts. 2015;**17**:552-560. DOI: 10.1039/C4EM00678J

[31] Moulder F, Sticke WF, Sobol PE, Bombel KD, Castain J, editors. Handbook of X-ray Photoelectron Spectroscopy. 2nd ed. Waltham, USA: Perkin-Elmer Corporation, Physical Electron Division; 1992. DOI: 10.1002/sia.740030412

[32] González L, Longoria-Rodríguez F, Sánchez-Domínguez M, Leyva-Porras C, Acuña-Askar K, Kharissov B, et al. Seasonal variation and chemical composition of particulate matter: A study by XPS, ICP-AES and sequential microanalysis using Raman with SEM/EDS. Journal of Environmental Sciences. 2018;**74**:32-49. DOI: 10.1016/j.jes.2018.02.002

[33] Thorpe A, Harrison RM. Sources and properties of non-exhaust particulate matter from road traffic: A review. Science of the Total Environment. 2008;**400**:270-282. DOI: 10.1016/j.scitotenv.2008.06.007

[34] Kelly F, Fussell J. Size, source and chemical composition as determinants of toxicity attributable to ambient particulate matter. Atmospheric Environment. 2012;**60**:504. DOI: 10.1016/j.atmosenv.2012.06.039

[35] Chen H, Laskin A, Baltrusaitis J, Gorski CA, Scherer MM, Grassian VH. Coal fly ash as a source of iron in atmospheric dust. Environmental Science & Technology. 2012;**46**(4):2112-2120. DOI: https://www.dora.lib4ri.ch/eawag/islandora/object/eawag:7063

[36] Kukutschová J, Moravec P, Tomásek V, Matejka V, Smolík J, Schwarz J, et al. On airborne nano/micro-sized wear particles released from low-metallic automotive brakes. Environmental Pollution. 2011;**159**:998-1006. DOI: 10.1016/j.envpol.2010.11.036

[37] Cherkezova-Zheleva Z, Paneva D, Kunev B, Kolev H, Shopska M, Nedkov I. Challenges at characterization of particulate matter—A case study. Bulgarian Chemical Communications. 2018;**50F**:93-98. DOI: http://www.bcc.bas.bg/index.html

[38] Schlesinger P, Mamane Y, Grishkan I. Transport of microorganisms to Israel during Saharan dust events. Aerobiologia. 2006;**22**:259-273. DOI: 10.1007/s10453-006-9038-7

[39] Maki T, Puspitasari F, Hara K, Yamada M, Kobayashi F, Hasegawa H, et al. Variations in the structure of airborne bacterial communities in a downwind area during an Asian dust (Kosa) event. Science of the Total Environment. 2014;**488-489**:75-84. DOI: 10.1016/j.scitotenv.2014.04.044

[40] De Nuntiis P, Maggi O, Mandrioli P, Ranalli G, Sorlini C. Monitoring the biological aerosol. In: Madrioli P, Caneva G, Sabbioni C, editors. Cultural Heritage and Aerobiology. Dordrecht: Kluwer Academic Publishers; 2003. pp. 107-144. ISBN: 978-94-017-0185-3

[41] Davies A, Thomson G, Walker J, Bennett A. A review of the risks and disease transmission associated with aerosol generating medical procedures. Journal of Infection Prevention. 2009;**10**(4):122-126. DOI: 10.1177/1757177409106456

[42] Després VR, Huffman JA, Burrows SM, Hoose C, Safatov AS, Buryak G, et al. Primary biological aerosol particles in the atmosphere: A review. Tellus B: Chemical and Physical Meteorology. 2012;**64**(1):2-20. DOI: 10.3402/tellusb.v64i0.15598

[43] Jones RM, Brosseau LM. Aerosol transmission of infectious disease. Journal of Occupational and Environmental Medicine. 2015;**57**(5):501-508. DOI: 10.1097/JOM.0000000000000448

[44] Ijaz MK, Zargar B, Wright KE, Rubino JR, Sattar SA. Generic aspects of the airborne spread of human

pathogens indoors and emerging air decontamination technologies. American Journal of Infection Control. 2016;**44**(9 Suppl):S109-S120. DOI: 10.1016/j.ajic.2016.06.008

[45] Griffin DW, Kubilay N, Kocak M, Gray MA, Borden TC, Kellogg CA, et al. Airborne desert dust and aeromicrobiology over the Turkish Mediterranean coastline. Atmospheric Environment. 2007;**41**:4050-4062. DOI: 10.1016/j.atmosenv.2007.01.023

[46] Kellogg CA, Griffin DW, Garrison VH, Peak KK, Royall N, Smith RR, et al. Characterization of aerosolized bacteria and fungi from desert dust events in Mali, West Africa. Aerobiologia. 2004;**20**:99-110. DOI: 10.1023/B:AERO.0000032947.88335.bb

[47] Akerman M, Valentine-Maher S, Rao M, Taningco G, Khan P, Tuysugoglu G, et al. Allergen sensitivity and asthma severity at an inner city asthma center. The Journal of Asthma. 2003;**40**(1):55. DOI: 10.1081/JAS-120017207

[48] Shinn EA, Smith GW, Prospero JM, Betzer P, Hayes ML, Garrison V, et al. African dust and the demise of Caribbean coral reefs. Geophysical Research Letters. 2000;**27**(19):3029-3032. DOI: 10.1029/2000GL011599

[49] Weir-Brush JR, Garrison VH, Smith GW, Shinn EA. The relationship between gorgonian coral (Cnidaria: Gorganacea) diseases and African dust storms. Aerobiologia. 2004;**20**(2):119-126. DOI: 10.1023/B:AERO.0000032949.14023.3a

[50] Wilken JA, Sondermeyer G, Shusterman D, McNary J, Vugia DJ, McDowell A, et al. Coccidioidomycosis among workers constructing solar power farms, California, USA, 2011-2014. Emerging Infectious Diseases. 2015;**21**(11):1997-2005. DOI: 10.3201/eid2111.150129

[51] Haig CW, Mackay WG, Walker JT, Williams C. Bioaerosol sampling mechanisms, bioefficiency and field studies. The Journal of Hospital Infection. 2016;**93**(3):242-255. DOI: 10.1016/j.jhin.2016.03.017

[52] Tang JW. The effect of environmental parameters on the survival of airborne infectious agents. Journal of the Royal Society Interfac. 2009;**6**(Suppl):S737-S746. DOI: DOI. 10.1098/rsif.2009.0227.focus

[53] Peccia J, Werth HM, Miller S, Hernandez. Effects of relative humidity on the ultraviolet induced inactivation of airborne bacteria. Aerosol Science and Technology. 2001;**35**(3):728-740. DOI: 10.1080/02786820152546770

[54] Won E, Ross H. Reaction of Airborne Rhizobium meliloti to some environmental factors. Applied Microbiology. 1969;**18**:556-557

[55] Tsai FC, Macher JM. Concentrations of airborne culturable bacteria in 100 large US office buildings from the BASE study. Indoor Air. 2005;**15**(Suppl 9):71-81. DOI: 10.1111/j.1600-0668.2005.00346

[56] Viegas C, Viegas S, Gomes A, Täubel M, Sabino R, editors. Exposure to Microbiological Agents in Indoor and Occupational Environments. 1st ed. Springer International Publishing AG; 2017. 415 p. DOI: 10.1007/978-3-319-61688-9

[57] Tang W, Kuehn TH, Simcik MF. Effects of temperature, humidity and air flow on fungal growth rate on loaded ventilation filters. Journal of Occupational and Environmental Hygiene. 2015;**12**(8):525-537. DOI: 10.1080/15459624.2015.1019076

[58] zur Nieden HA, Jankofsky M, Stilianakis NI, Boedeker R-H, Eikmann TF. Effects of bioaerosol polluted outdoor air on airways of residents:

A cross sectional study. Occupational and Environmental Medicine. 2003;**60**(5):336-342. DOI: 10.1136/oem.60.5.336

[59] Kellogg CA, Griffin DW. Aerobiology and the global transport of desert dust. Trends in Ecology & Evolution. 2006;**21**(11):638-644. DOI: 10.1016/j.tree.2006.07.004

[60] Bragoszewska E, Mainka A, Pastuszka JS. Concentration and size distribution of culturable bacteria in ambient air during spring and winter in Gliwice: A typical urban area. Atmosphere. 2017;**8**(12):239-252. DOI: 10.3390/atmos8120239

[61] Shivaji S, Chaturvedi P, Suresh K, Reddy GS, Dutt CB, Wainwright M, et al. *Bacillus aerius* sp. nov., *Bacillus aerophilus* sp. nov., *Bacillus stratosphericus* sp. nov. and *Bacillus altitudinis* sp. nov., isolated from cryogenic tubes used for collecting air samples from high altitudes. International Journal of Systematic and Evolutionary Microbiology. 2006;**56**(Pt 7):1465-1473. DOI: 10.1099/ijs.0.64029-0